powders

MDPI

Article

Direct Powder Forging—A New Approach for near Net Shape Processing of Titanium Powders

Sébastien Germain Careau *, Elena Ulate-Kolitsky and Bernard Tougas

Centre de Métallurgie du Québec, 3095 rue Westinghouse, Trois-Rivières, QC G9A 5E1, Canada
* Correspondence: sebastien.germain.careau@cegeptr.qc.ca

Abstract: This study investigates direct powder forging (DPF) as a new approach for near-net-shape processing of titanium alloys using a coarse particle size distribution (PSD) between 90 and 250 µm. This route was utilised to takes advantage of DPF's enclosed nature to make near-net-shape components with conventional forging equipment, making it attractive and viable even for reactive powder such as titanium. In this study, the uncompacted Ti-6Al-4V ELI powder was sealed under vacuum in a stainless-steel canister and hot forged in air to produce a fully dense titanium femoral stem. After the final forging stage, the excess material in the flash region was cut, which efficiently released the canister, revealing the forged part with minimal surface contamination. The as-forged microstructure comprises coarse β grains with a martensitic structure. The subsequent annealing was able to generate a fine and homogenous lamellar microstructure with mechanical properties that respects the surgical implant standard, showing that DPF offers significant potential for forged titanium parts. Therefore, the DPF process provides a suitable alternative to produce titanium components using basic equipment, making it more available to the industry.

Keywords: direct powder forging; near-net-shape; titanium alloy; biomedical application; microstructure evaluation; mechanical properties

check for updates

Citation: Germain Careau, S.; Ulate-Kolitsky, E.; Tougas, B. Direct Powder Forging—A New Approach for near Net Shape Processing of Titanium Powders. *Powders* **2023**, *2*, 21–31. https://doi.org/10.3390/powders2010002

Academic Editor: Paul F. Luckham

Received: 13 October 2022
Revised: 1 December 2022
Accepted: 20 December 2022
Published: 4 January 2023

1. Introduction

Titanium alloys play an important role in the aerospace [1], automotive [2] and biomedical industries [3,4]. Yet, titanium's requirement for a controlled atmosphere during its production and processing make titanium mill products very expensive [5]. The search for viable alternatives to replace mill products and to reduce machining of the billet has been a topic of great interest.

Powder metallurgy (PM) has the potential to do both. PM has been used for the consolidation of fully dense parts using titanium powder robust PM techniques such as vacuum sintering [6] and hot isostatic pressing (HIP) [7,8]. However, both processes are lengthy and energy intensive, which contributes to the high cost of the final product [9]. More novel approaches have been reported to generate fully dense samples with comparable properties to wrought alloys [10]. For example, induction sintering [6], spark plasma sintering (SPS) [11], extrusion [12,13], FAST-forge (Field-assisted sintering technology) [14] and direct powder forging (DPF) [15–17]. In the case of SPS [18] and FAST-forge [19], both have been shown to achieve near-net shape (NNS) parts with complex geometries. DPF has been proposed for processing nickel-based superalloys, but only simple cylindrical shapes have been achieved [20,21]. Furthermore, all experiments conducted on the DPF of titanium-based alloys were designed for simple rectangular bars to investigate microstructural and mechanical behavior [15].

DPF and FAST-forge are new PM forging techniques that have the potential to consolidate powder into NNS components by close-die forging, which makes them attractive to the industries. Moreover, they both provide limited pick-up of impurities (C, O, N) and have the ability to utilize various feedstock, such as coarse spherical and angular powders.

FAST-forge has already been reported to produce simple geometries at the laboratory scale (Ti-6Al-4V) [14] and the industrial scale (β-Ti alloy) [22]. Additionally, closed-die forging of NNS components was achieved starting from a FAST-forged preform of dissimilar titanium alloy [23]. Meanwhile, DPF has only been used to generate mill-like rods, which have proven comparable to commercially available [15,24]. However, DPF has the significant advantage of only needing standard forging equipment compared with FAST-forge, which requires SPS to produce the preform. Indeed, with DPF, only conventional presses and heating sources, such as the one used for the steel industry, are needed to process canister encapsulated titanium powder to achieve the desired form. Moreover, the loose powder thermomechanical processing of DPF avoids the conventional compaction and sintering steps in standard PM. Thus, DPF pushes further the key strategy to reduce the processing steps to produce more cost-effective titanium parts [9].

The aim of the present work was to demonstrate, at a laboratory scale, that DPF is a viable technology to produce NNS components by producing a Ti-6Al-4V ELI femoral stem implant with closed-die forging that respects the ASTM F136-13 (2021) standards [25]. In addition, the study wants to demonstrate that DPF can utilize coarse powders with a large particle size distribution (PSD). Thus, reducing the environmental footprint by utilizing off-cuts powders that are usually discarded.

2. Materials and Methods

2.1. Materials

The DPF process of femoral stem implants was done using a pre-alloyed Tekna Advanced Materials plasma atomized Ti-6Al-4V (Grade 23) spherical powder. The particles chemical composition, average size and morphology of the base powder are presented in Table 1 and Figure 1. These large spherical particles are offcuts from their standard production; their market mostly being the additive manufacturing sector.

Table 1. Chemical composition and average size of the base powder.

	Chemical Composition [%-wt.]							**Size**
	Ti	Fe	Al	V	O	N	C	D_{50} (µm)
Ti-6Al-4V	Bal.	0.16	6.43	4.15	0.04	0.01	<0.01	150

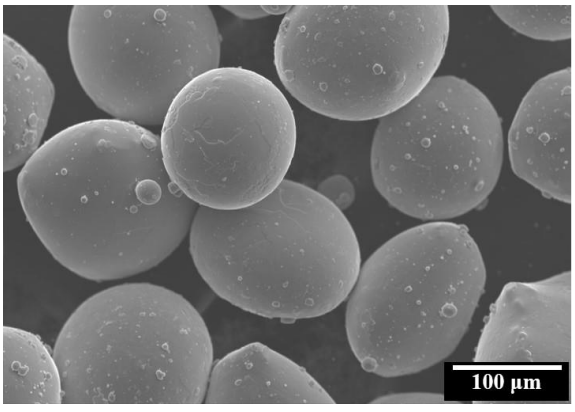

Figure 1. SEM micrograph presenting the size and shape of the base powder.

Sanitary grade 316L stainless steel (CFF Stainless Steels Inc., Montreal, QC, Canada) has been shown to have excellent formability at high temperature, which is an important criterion for the near-net-shape process using DPF [26]. Therefore, the latter was selected to fabricate the enclosed canisters. The dimensions of the starting canister were 38.1 mm for the outer diameter, 88.9 mm for the total length. The tube wall thickness was 1.3 mm.

2.2. Forming Process

The investigated NNS process, which aimed to produce femoral stem implants using DPF, consisted of three major steps. The sequence starts by preparing the enclosed canister and it is followed by the primary forging of the bar. Thus, the powder was poured into the stainless-steel canister and sealed under a vacuum of 0.4 Pa. The sealed stainless-steel container was than heated up to 1000 °C for 3 h to ensure initial bonding between particles. The following forging and rolling step were done in air at 1100 °C to produce a rectangular bar. A total of 50% deformation was performed to achieve the desired dimension. At this stage, the forged rectangular bar has a cross section of 20 mm × 20 mm and a length of 150 mm. Following the primary forging stage, the preform is made by tapering one end and bending the bar to match the curvature of the femoral stem. Finally, the final precision forging is performed in a single closed-die step. Boron nitride coating was applied onto the die surface to reduce friction and avoid adherence. In this study, a conventional single-action hydraulic press with a maximum forging pressure of 1226 kN and a forming velocity of 20 mm/s was utilized (CMQ, Trois-Rivières, QC, Canada). After the final precision forging step, the excess material in the flash region was cut-out at room temperature to avoid oxidation of the part, which efficiently released the stainless-steel canister. Indeed, as it was presented in a previous study about the DPF of titanium alloys [15,24], intermetallics are formed at the canister-alloy interface. These brittle compounds fracture during the DPF thermomechanical steps, limiting the bonding between the stainless-steel and the titanium alloy. After canister removal, the forged titanium part was annealed in vacuum at 800 °C for 2 h and then furnace cooled. Figure 2 presents a schematic representation of the NNS process employed in this study to process titanium powder into femoral stem implant by DPF. As for Figures 3 and 4, they, respectively present the outcome at each stage of the process and the forged femoral stem with the cut-out canister shell. The latter demonstrates the easy canister removal of the titanium DPF process. It can also be seen that the DPF femoral stem exhibits slight surface oxidation, which was caused by the rupture of the canister during the final forging step. Minor adjustments to the forging sequence and die design can resolve this issue. Nevertheless, as it will be shown later, this slight contamination did not affect the mechanical properties of the NNS parts.

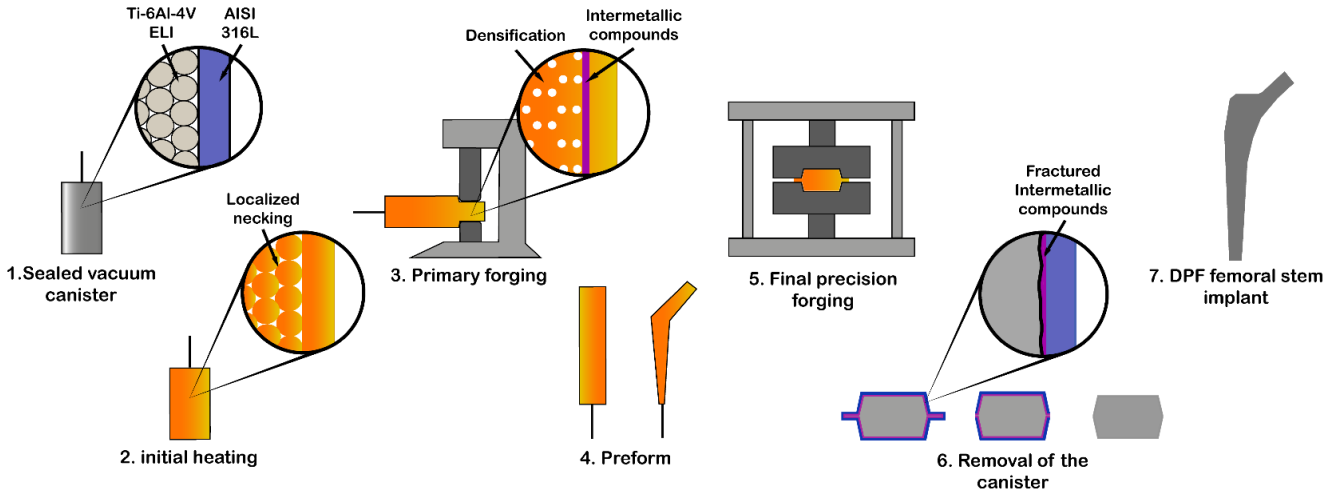

Figure 2. Schematic representation of the DPF NNS procedure used in this study to process titanium powder into femoral stem implant.

Figure 3. From left to right, photographs presenting the initial canister, the forged billet, the preform, the final precision forging, the cut-out sample and the sandblasted final component.

Figure 4. Photograph presenting the simple canister removal. The cut-out sample (**left**) and the canister shell (**right**).

Density of the DPF component was measured with the Archimedes principle following the ASTM B962-17 standard [27]. Chemical composition was measured with a Thermo Scientific (ARL 3460 Metals Analyzer, Thermo Fisher Scientific Inc, Mississauga, ON, Canada) on the annealed specimens in accordance with the ASTM E2371-21a [28]. The microstructure was observed on the component cross-sections at three different locations (Body, Neck and Tapered stem). Samples were polished to a 0.05 µm surface finish and etched with a solution of 2%-vol. HF and 5%-vol. H_2O_2 mixed in distilled water. Observations were made with a Keyence VHX-7000 series digital microscope (Keyence Canada inc., Mississauga, ON, Canada) and a Hitachi SU3500 scanning electron microscope (SEM, Hitachi High-Technologies Corporation, Tokyo, Japan). Rockwell C hardness was measured on the as-forged and heat-treated samples cross-section at the same locations with a Clark Instrument CR series Rockwell type hardness tester (Sun-Tec Corporation, Novi, MI, USA). Crystal structures and texture intensities were determined by X-Ray diffraction with a Bruker D8 X-Ray powder diffractometer equipped with a CuKα source (Bruker Elemental GmbH, Kalkar, Germany). Lastly, the tensile properties were evaluated with a strain rate of 0.015 mm/mm/min using an MTS Exceed E43 machine (MTS System, Eden Prairie, MN, USA). Thread ends rounded tensile samples were prepared following the ASTM E8/E8M-21 standard [29]. Figure 5 shows the sampling locations for the hardness, micrographs and tensile specimens.

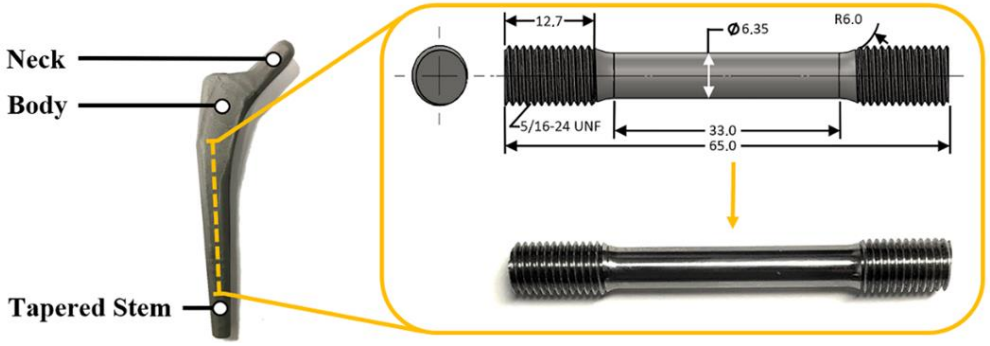

Figure 5. Detail view of the tensile bar and sampling locations for hardness, micrographs and tensile specimens.

3. Results and Discussion

3.1. Physical Properties

The average titanium femoral stem density is presented in Table 2. Full densification was obtained with the DPF process. A previous study demonstrated that the primary forging of the bar ingot yielded fully dense parts, which was needed in the forging of the femoral stem [15]. Therefore, the final forming step only created the desired shape, leading to fully dense PM titanium femoral stem elaborated from coarse powder.

Table 2. Average density of the femoral stem produces via NNS DPF process.

	Density (g/cm^3)		**Relative Density (%)**
	Theoretical	Measured	
Ti-6Al-4V$_{DPF}$	4.430	4.425 ± 0.005	99.9

3.2. Chemical Composition

Table 3 presents the OES chemical composition of the annealed NNS stem. The results show no significant variation from the starting composition. The Ti-6Al-4V$_{DPF}$ iron content was not increased due to the presence of the canister. Overall, the composition respects the ASTM F136-13 (2021) standard specification for Ti-6Al-4V ELI used for Surgical Implants [25]. Moreover, the authors have presented in previous work that surface chemical variation occurs at the titanium alloy surface resulting from the diffusion at the canister-alloy interface [15]. Mainly iron (Fe), chromium (Cr) and nickel (Ni) were measured within 100 µm of the Ti-6Al-4V alloy. In this work, further processing steps required for the NNS of the femoral stem have engendered higher surface contamination (Figure 6). Still, the diffusion is limited to 200 µm of the surface which can be further removed using chemical roughening surface methods, giving better biocompatibility [30].

Table 3. Average OES chemical analysis of the produced NNS stems.

	Chemical Composition [%-wt.]						
	Ti	Fe	Al	V	O	N	C
Ti-6Al-4V$_{DPF}$	Bal.	0.16	6.43	4.15	0.04	0.01	<0.01
ASTM F136 STD	Bal.	0.25	5.5–6.5	3.5–4.5	0.13	0.05	0.08

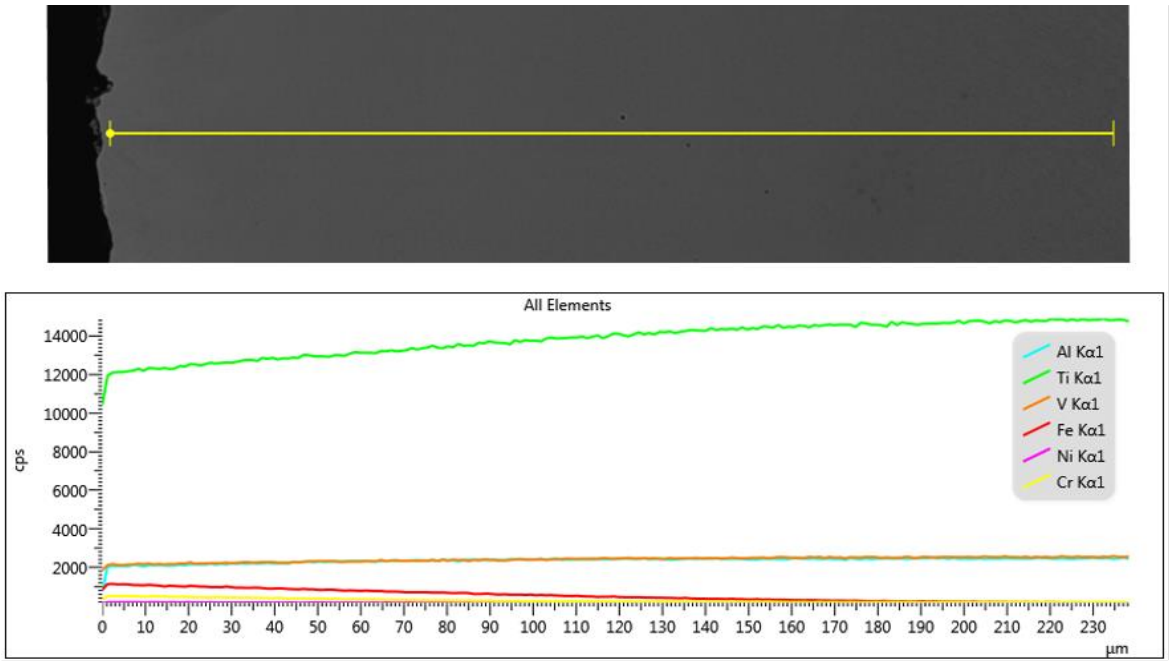

Figure 6. EDS linescan of the contamination at the Ti-6Al-4V_{DPF} femoral stem surface.

3.3. Phase Identification

The XRD patterns of the as-DPF and heat-treated DPF femoral stem are presented in Figure 6. The primary phase for both samples is a titanium α-phase, preferred orientation was noted on the (0 0 2) alpha-peaks. The texture can be attributed to the final single step unidirectional close-die forging. Although the sample was annealed at 800 °C the preferred orientation remains. Regarding the β-phase, no clear β peak was identified in the as-DPF sample, it is important to point out a slight broadening of the (1 0 1) alpha-peak which could be evidence of some remaining β-phase that did not transform into martensite during the rapid cooling from the forging [31], see detailed view in Figure 7's upper right corner. Although we cannot affirm the existence nor absence of the β-phase by XRD analysis, a further microstructural examination was needed to correlate the XRD evidence. The latter is described in detail in the next section. Additionally, the β-phase formed after the annealing corresponds to the typical martensitic decomposition into a stable α + β microstructure [32].

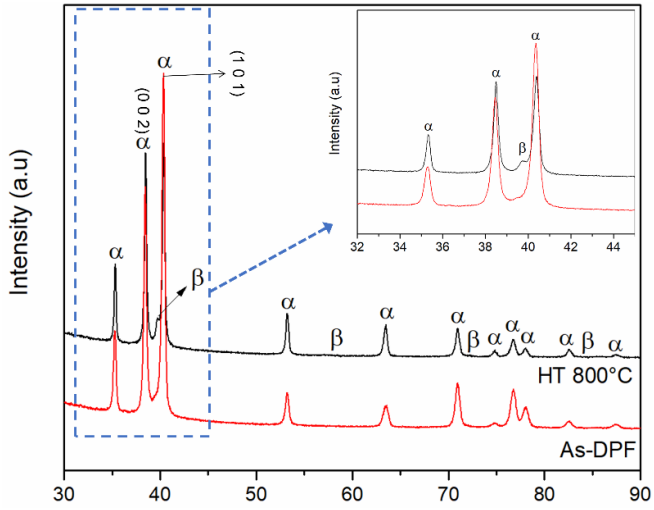

Figure 7. XRD pattern of the DPF femoral stem in the as-forged and heat-treated conditions.

3.4. Microstructures of the As-Forged Femoral Stem

The femoral stem has distinct sections of various thicknesses and geometry, leading to a difference in material deformation and cooling rates throughout the close-die forging step. Therefore, microstructure analysis was carried out at different locations, corresponding to the neck, body and tapered stem (Figure 5). As it can be observed in Figure 8, coarse grains with an equiaxed morphology are present at the surface of all three regions. Large grains are expected since the entire DPF process leading to the final forging stage was performed at high temperatures with low deformation rates. Each region exhibits a distinct grain evolution between the surface and the core. At the center, the micrographs show elongated grain perpendicular to the forging axis for the body and tapered stem regions. This microstructural aspect indicated that a preferential deformation orientation, typical of upsetting forging, had governed the deformation mechanism in those regions. On the other hand, the neck region exhibited an entire equiaxed grain microstructure and almost no sign of elongation at the core. This microstructure suggests that β grains recrystallization and growth were favored by the local deformations that are conditioned by the round morphology of the neck region.

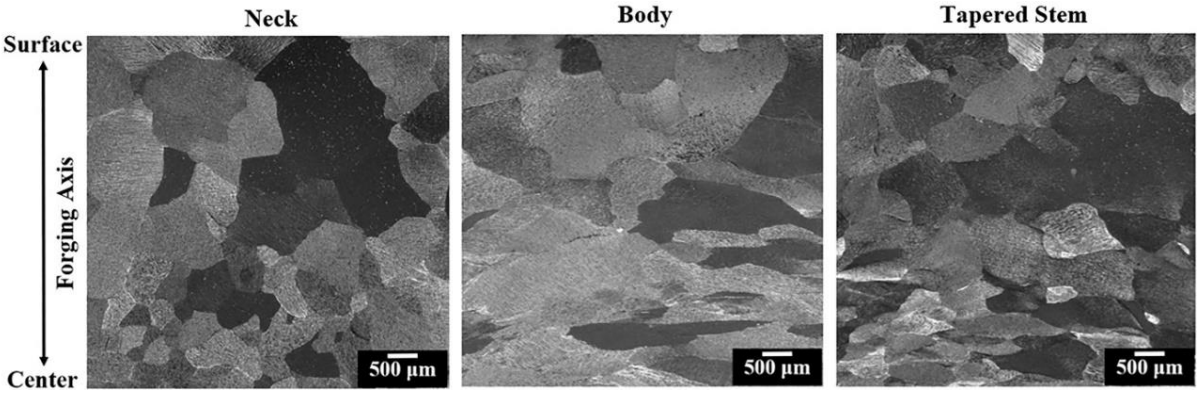

Figure 8. Digital micrograph showing the grains size and morphology of the prior β-grain of the as-DPF femoral stem at the three locations.

As it was mentioned, recrystallization was only observed in the core of the neck region. The utilization of a low strain rate during β-phase forging is likely to generate more dynamic recovery (DRV) than dynamic recrystallization (DRX) because, the high self-diffusivity of β-Ti and the decreasing store energy favor easier deformation but lower recrystallization [33–37]. During the final precision forging stage, high heat transfer from the dies allowed for a rapid cooling at the sample surface, which created a temperature gradient with the core. Therefore, the deformation mainly occurred at the center and has generated deformation banding in the body and tapered stem region. Additionally, the more refined microstructure at the tapered stem than in the body region indicates a more severe deformation for this location. The heterogeneous coarse grain's structure is not ideal for titanium components, thus optimization of the process parameters, die design and the forming sequence can be further investigated in the future to uniformized and refine the structure.

As presented in Figure 9, the martensitic microstructure was observed in all areas of interest. No significant difference was found between the surface and the center in all regions of the as-forged femoral stem. The martensite formation indicated that the cooling rate in the final forging stage was high enough to reach T_{Ms} and prevented formation of diffusional controlled microstructures, such as the Widmanstätten α. The die chilling and the low velocity single-action hydraulic press were responsible for the fast-cooling. Therefore, the martensitic α′ phase, composed of orthogonal and parallel acicular plates, has nucleated at the prior β-grain boundaries and grows within the grain giving its distinguishing features, typical of the martensitic structure of titanium alloys [38,39].

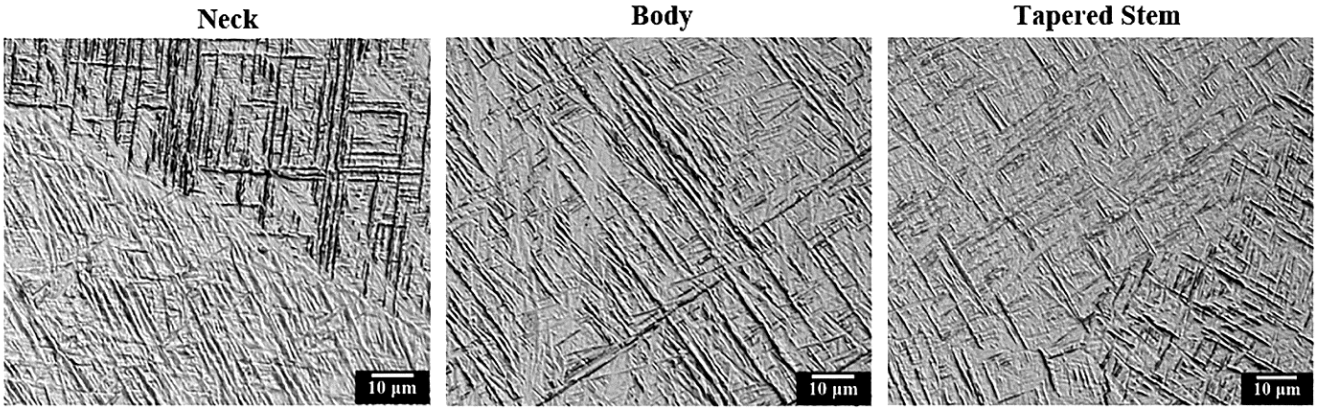

Figure 9. Digital micrograph of the martensite at the different locations of the DPF femoral stem.

3.5. Effect of Heat Treatment on Microstructure and Mechanical Properties

The microstructures of the heat-treated Ti-6Al-4V$_{DPF}$ femoral stem show that there was no significant modification to the grain size or their morphology. As shown in Figure 10, the prior β-grain remained elongated and similar to the as-forged condition for the body and tapered stem regions. As mentioned by Gil and Planell [40], a heat treatment below the β-transus temperature has small effect on grains growth and recrystallization. Therefore, no recrystallization was observed, and the grain size remained coarse after the heat treatment. Annealing in the α + β phase region was carried out to modify the martensite, thus the microstructure exhibits a significant change. The martensitic decomposition has occurred during the annealing, resulting in a stable mixture of α + β phase. Precipitation of the β phase and the depletion of the α′ phase has engendered a fine lamellar structure (Figure 11). Furthermore, after forging, the various sections of the femoral stem exhibit different hardness (Table 4). The grain size is likely to cause this variation in hardness, giving the tapered stem the highest value while the body exhibits the lowest hardness [38]. Nevertheless, annealing of the forged part homogenized the hardness in every region of the femoral stem.

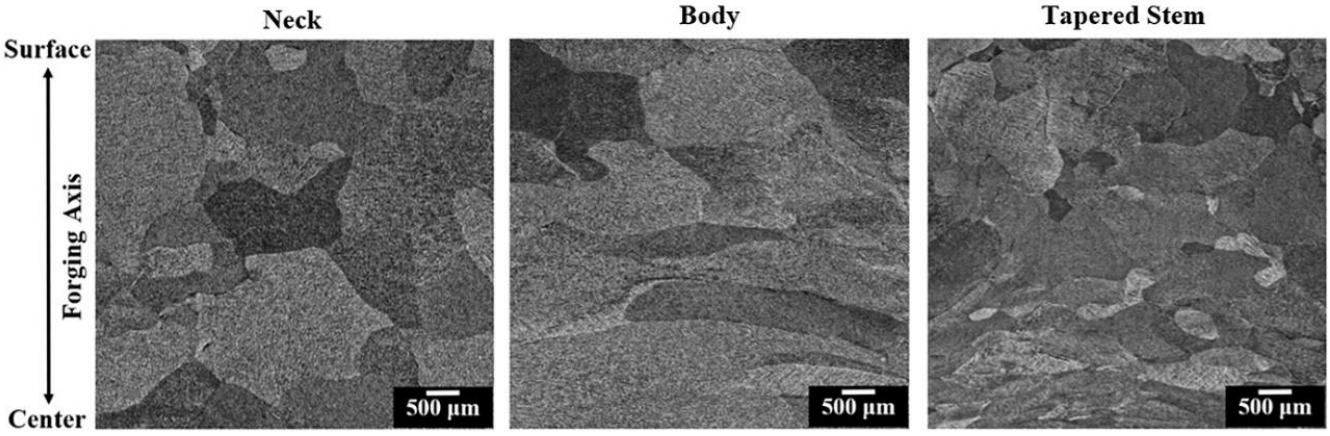

Figure 10. Digital micrograph showing the grains size and morphology of the prior β grain after annealing heat-treatment.

Table 4. Average HRC hardness of the as-forged and heat-treated conditions for each region of interest of the Ti-6Al-4V$_{DPF}$ ELI hip component.

	Neck	Body	Tapered Stem
As-forged	34.7 ± 0.4	33.7 ± 0.2	36.6 ± 0.5
HT 800 °C	34.6 ± 0.1	34.6 ± 0.3	34.8 ± 0.3

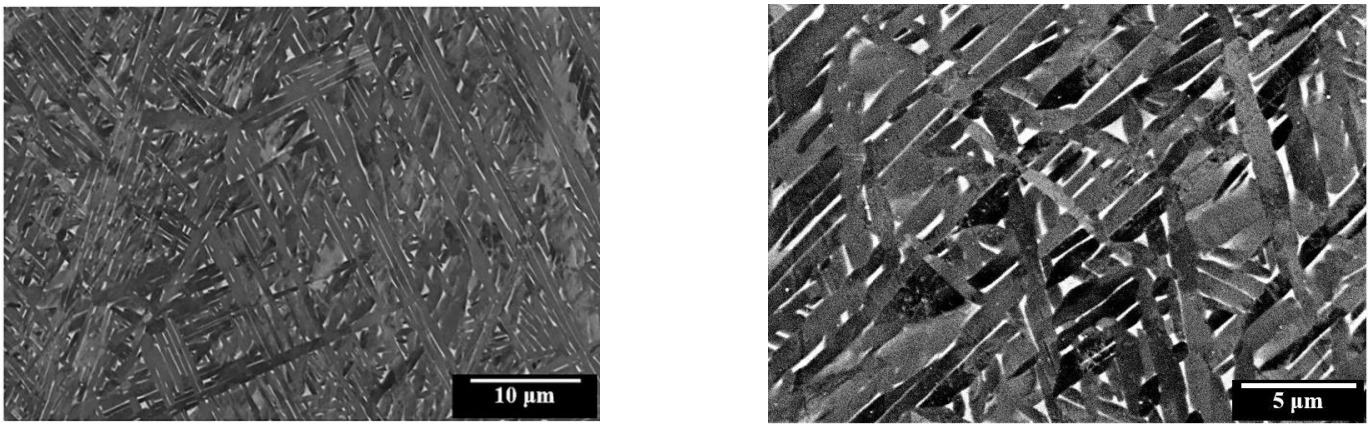

(**a**) (**b**)

Figure 11. (**a**) Typical SEM micrograph of the heat-treated titanium femoral stem produced via DPF showing the α + β lamella microstructure; (**b**) Higher magnification showing the fine lamella morphology.

The tensile properties of the DPF femoral stem in the forged and annealed condition are presented in Figure 12. Average mechanical properties reaching 926 MPa for yield strength, 994 MPa for ultimate tensile strength and 10.7% for elongation were obtained. Results have attractive potential for medical application greatly exciding the required strength of the ASTM F136-13 (2021) standard [25] (Y.S 795 MPa, UTS 860 MPa, El 10%). If required, higher ductility could have been obtained by increasing the annealing temperature. As it was mentioned, it is well known that large grains are not optimal for forged components that require good tensile properties. Nonetheless, the authors previously reported that noteworthy mechanical properties combining tensile strength with high ductility were obtained via the DPF method for a coarse grain lamellar microstructure [15]. It is, however, important to state that, depending on the application, optimizing the process parameters such as the forging temperature, strain rate and post-production heat treatment are valuable aspects that can significantly modify the microstructure, tailoring the mechanical properties for a given applications.

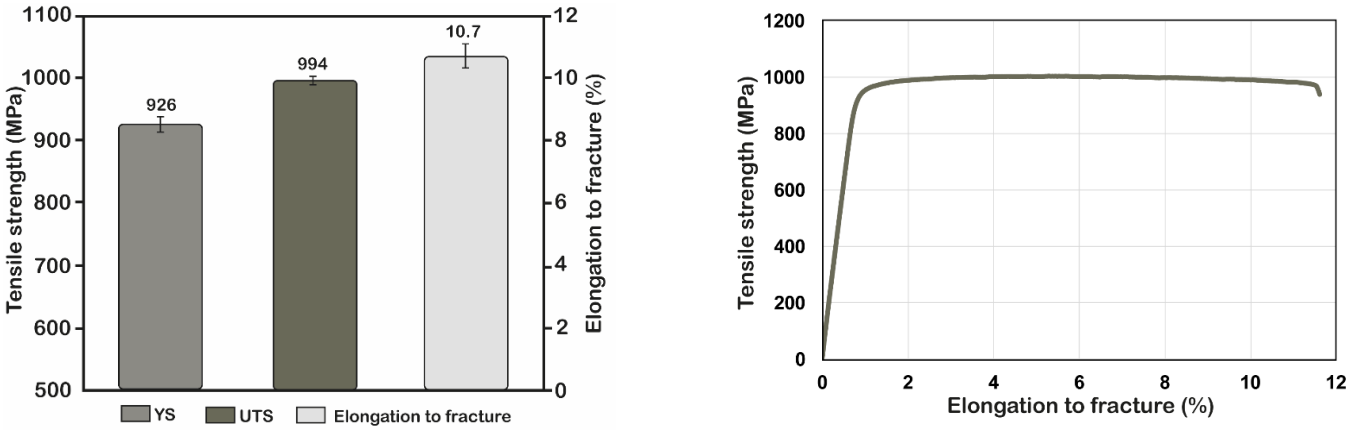

(**a**) (**b**)

Figure 12. (**a**) Average YS, UTS and elongation to fracture of the DPF and heat-treated Ti-6Al-4V$_{DPF}$ femoral stem; (**b**) Representative stress–strain curve.

4. Conclusions

The study evaluated DPF as a new approach for near-net-shape titanium powder processing. It was demonstrated, at the laboratory scale, that a fully dense titanium femoral stem implant can be made using loose and enclosed titanium powder with a PSD between

90 and 250 μm. The proposed method shows that basic steel forging equipment can be used, which makes this process more accessible to the market. It also indicates that DPF can reduce the processing steps by avoiding the conventional press and sinter or HIP method, providing possibilities for a more effective and viable process.

The microstructural analysis shows that the as-forged Ti-6Al-4V alloy exhibits a fully martensitic and coarse grain microstructure. No distinctive microstructural features were observed relative to the conventional forging of Ti-6Al-4V alloy, which indicated a good forging behavior during DPF. The subsequent annealing engendered a fine and homogenous lamellar microstructure with mechanical properties respecting the ASTM F136-13 (2021) standard specification for biomedical Ti-6Al4V ELI parts. It is believed that further appropriate adjustment of the forging sequence and parameters, as well as the post-forging heat treatment, can even further improve the mechanical properties of the Ti-6Al-4V$_{DPF}$ parts by decreasing the β grain size.

Author Contributions: Conceptualization, S.G.C. and B.T.; methodology, S.G.C.; investigation, S.G.C. and E.U.-K.; writing—original draft preparation, S.G.C. and E.U.-K.; writing—review and editing, S.G.C., B.T. and E.U.-K.; visualization, S.G.C.; supervision, B.T.; project administration, B.T. All authors have read and agreed to the published version of the manuscript.

Funding: This research received no external funding.

Institutional Review Board Statement: Not applicable.

Informed Consent Statement: Not applicable.

Data Availability Statement: Not applicable.

Acknowledgments: The authors would like to acknowledge the support given by the Centre de Métallurgie du Québec (CMQ). The research was performed at the Centre de Métallurgie du Québec (CMQ).

Conflicts of Interest: The authors declare no conflict of interest.

References

1. Liu, Z.; He, B.; Lyu, T.; Zou, Y. A Review on Additive Manufacturing of Titanium Alloys for Aerospace Applications: Directed Energy Deposition and beyond Ti-6Al-4V. *JOM* **2021**, *73*, 1804–1818. [CrossRef]
2. Wollmann, M.; Kiese, J.; Wagner, L. Properties and Applications of Titanium Alloys in Transport. In *Ti-2011*; Zhou, L., Chang, H., Lu, Y., Xu, D., Eds.; Science Press Beijing: Beijing, China, 2011; pp. 837–844.
3. Popovich, A.; Sufiiarov, V.; Polozov, I.; Borisov, E.; Masaylo, D. Producing hip implants of titanium alloys by additive manufacturing. *Int. J. Bioprint.* **2016**, *2*, 78–84. [CrossRef]
4. Kaur, M.; Singh, K. Review on titanium and titanium based alloys as biomaterials for orthopaedic applications. *Mater. Sci. Eng. C* **2019**, *102*, 844–862. [CrossRef]
5. Kraft, E.H. Summary of Emerging Titanium Cost Reduction Technologies. In *A Study Performed for US Department of Energy and Oak Ridge National Laboratory Subcontract 4000023694*; EHK Technologies: Vancouver, WA, USA, 2004.
6. Raynova, S.; Yang, F.; Bolzoni, L. Mechanical behaviour of induction sintered blended elemental powder metallurgy Ti alloys. *Mater. Sci. Eng. A* **2020**, *799*, 140157. [CrossRef]
7. Fang, Z.Z.; Paramore, J.D.; Sun, P.; Chandran, K.S.R.; Zhang, Y.; Xia, Y.; Cao, F.; Koopman, M.; Free, M. Powder metallurgy of titanium—past, present, and future. *Int. Mater. Rev.* **2017**, *63*, 407–459. [CrossRef]
8. Zhang, C.; Pan, Y.; Sun, J.; Lu, X.; Zhang, J. A net-shape forming process of Ti–6Al–4V sphere joints. *Powder Met.* **2021**, *64*, 404–411. [CrossRef]
9. Bodunrin, M.O.; Chown, L.H.; Omotoyinbo, J.A. Omotoyinbo. Development of low-cost titanium alloys: A chronicle of challenges and opportunities. *Mater. Today Proc.* **2021**, *38*, 564–569. [CrossRef]
10. Oke, S.R.; Ogunwande, G.S.; Onifade, M.; Aikulola, E.; Adewale, E.D.; Olawale, O.E.; Ayodele, B.E.; Mwema, F.; Obiko, J.; Bodunrin, M.O. An overview of conventional and non-conventional techniques for machining of titanium alloys. *Manuf. Rev.* **2020**, *7*, 34. [CrossRef]
11. Zhang, W.; Yang, P.; Cao, Y.; Li, X.; Wei, D.; Kato, H.; Wu, Z. New Ti/β-Ti alloy laminated composite processed by powder metallurgy: Microstructural evolution and mechanical property. *Mater. Sci. Eng. A* **2021**, *822*, 141702. [CrossRef]
12. Umeda, J.; Tanaka, T.; Teramae, T.; Kariya, S.; Fujita, J.; Nishikawa, H.; Shibutani, Y.; Shen, J.; Kondoh, K. Microstructures analysis and quantitative strengthening evaluation of powder metallurgy Ti–Fe binary extruded alloys with (α+β)-dual-phase. *Mater. Sci. Eng. A* **2021**, *803*, 140708. [CrossRef]
13. Niu, H.; Zhang, H.; Sun, Q.; Zhang, D. Breaking through the strength-ductility trade-off dilemma in powder metallurgy Ti–6Al–4V titanium alloy. *Mater. Sci. Eng. A* **2019**, *754*, 361–369. [CrossRef]

14. Weston, N.; Jackson, M. FAST-forge—A new cost-effective hybrid processing route for consolidating titanium powder into near net shape forged components. *J. Mater. Process. Technol.* **2017**, *243*, 335–346. [CrossRef]
15. Careau, S.G.; Tougas, B.; Ulate-Kolitsky, E. Effect of direct powder forging process on the mechanical properties and microstructural of Ti-6Al-4E ELI. *Materials* **2021**, *14*, 4499. [CrossRef]
16. Olsson, L.R.; Lampe, V.; Fischmeister, H. Direct forging of high-alloy steel powders to bar stock. *Powder Metall.* **1974**, *17*, 347–362. [CrossRef]
17. Jiang, J. Development of Direct Powder Forging Process. Ph.D. Thesis, Imperial College London, South Kensington, UK, 2017. [CrossRef]
18. Manière, C.; Lee, G.; Olevsky, E.A. All-Materials-Inclusive Flash Spark Plasma Sintering. *Sci. Rep.* **2017**, *7*, 15071. [CrossRef]
19. Childerhouse, T.; Jackson, M. Near net shape manufacture of titanium alloy components from powder and wire: A review of state-of-the-art process routes. *Metals* **2019**, *9*, 689. [CrossRef]
20. Bai, Q.; Lin, J.; Jiang, J.; Dean, T.; Zou, J.; Tian, G. A study of direct forging process for powder superalloys. *Mater. Sci. Eng. A* **2015**, *621*, 68–75. [CrossRef]
21. Wang, S.; Fang, S.; Shi, Z.; Jiang, J.; Zhou, X.; Lin, J. Direct powder forging of PM nickel-based superalloy: Densification and recrystallisation. *Int. J. Adv. Manuf. Technol.* **2017**, *88*, 2661–2670. [CrossRef]
22. Calvert, E.; Wynne, B.; Weston, N.; Tudball, A.; Jackson, M. Thermomechanical processing of a high strength metastable beta titanium alloy powder, consolidated using the low-cost FAST-forge process. *J. Mater. Process. Technol.* **2018**, *254*, 158–170. [CrossRef]
23. Pope, J.; Jackson, M. Fast-forge of diffusion bonded dissimilar titanium alloys: A novel hybrid processing approach for next generation near-net shape components. *Metals* **2019**, *9*, 654. [CrossRef]
24. Careau, S.G.; Ulate-Kolitsky, E.; Tougas, B. In-situ alloying of Ti-5Fe titanium alloy using direct powder forging and the effect of the powder mixing method. *Materialia* **2022**, *24*, 101471. [CrossRef]
25. *ASTM F136-21*; Standard Specification for Wrought Titanium 6Aluminium-4Vanadium ELI (Extra Low Interstitial) Alloy for Surgical Implant Applications (UNS R56401). ASTM International: West Conshohocken, PA, USA, 2018. Available online: www.astm.org (accessed on 22 July 2022).
26. Dharavath, B.; Haq, A.U.; Varma, M.D.; Buddi, T.; Singh, S.K.; Naik, M.T. Comparative study of ASS 316L on formability at room temperature and super plastic region. *Adv. Mater. Process. Technol.* **2020**, *6*, 384–395. [CrossRef]
27. *ASTM B962-17*; Standard Test Methods for Density of Compacted or Sintered Powder Metallurgy (PM) Products Using Archimedes' Principle. ASTM International: West Conshohocken, PA, USA, 2018. Available online: www.astm.org (accessed on 22 July 2022).
28. *ASTM E2371-21a*; Standard Test Method for Analysis of Titanium and Titanium Alloys by Direct Current Plasma and Inductively Coupled Plasma Atomic Emission Spectrometry (Performance-Based Test Methodology). ASTM International: West Conshohocken, PA, USA, 2018. Available online: www.astm.org (accessed on 22 July 2022).
29. *ASTM E8/E8M-21*; Standard Test Methods for Tension Testing of Metallic Materials. ASTM International: West Conshohocken, PA, USA, 2016. Available online: www.astm.org (accessed on 22 July 2022).
30. Bai, L.; Gong, C.; Chen, X.; Sun, Y.; Zhang, J.; Cai, L.; Zhu, S.; Xie, S.Q. Additive Manufacturing of Customized Metallic Orthopedic Implants: Materials, Structures, and Surface Modifications. *Metals* **2019**, *9*, 1004. [CrossRef]
31. Jaber, H.; Kónya, J.; Kulcsár, K.; Kovács, T. Effects of Annealing and Solution Treatments on the Microstructure and Mechanical Properties of Ti6Al4V Manufactured by Selective Laser Melting. *Materials* **2022**, *15*, 1978. [CrossRef]
32. Zhang, Z.; Qu, S.; Feng, A.; Shen, J. Achieving grain refinement and enhanced mechanical properties in Ti–6Al–4V alloy produced by multidirectional isothermal forging. *Mater. Sci. Eng. A* **2017**, *692*, 127–138. [CrossRef]
33. Guo, L.; Fan, X.; Yu, G.; Yang, H. Microstructure control techniques in primary hot working of titanium alloy bars: A review. *Chin. J. Aeronaut.* **2016**, *29*, 30–40. [CrossRef]
34. Semiatin, S.L. An Overview of the Thermomechanical Processing of α/β Titanium Alloys: Current Status and Future Research Opportunities. *Met. Mater. Trans. A.* **2020**, *51*, 2593–2625. [CrossRef]
35. Chatterjee, R.; Murty, S.V.S.N.; Alankar, A. Dynamic Recrystallization in Titanium Alloys: A Comprehensive Review. *Mater Perform. Charact.* **2020**, *9*, 1–42. [CrossRef]
36. Dong, Y.; Liu, X.; Zou, J.; Ke, Y.; Liu, P.; Ma, L.; Luo, H. Effect of Cooling Rate Following B Forging on Texture Evolution and Variant Selection during B$\rightarrow\alpha$ Transformation in Ti-55511 Alloy. *J. Mater. Sci. Technol.* **2022**, *113*, 1–13. [CrossRef]
37. Fan, X.G.; Yang, H.; Gao, P.F.; Zuo, R.; Lei, P.H. The Role of Dynamic and Post Dynamic Recrystallization on Microstructure Refinement in Primary Working of a Coarse Grained Two-Phase Titanium Alloy. *J. Mater. Process. Technol.* **2016**, *234*, 290–299. [CrossRef]
38. Motyka, M. Martensite Formation and Decomposition during Traditional and AM Processing of Two-Phase Titanium Alloys—An Overview. *Metals* **2021**, *11*, 481. [CrossRef]
39. Ahmed, T.; Rack, H.J. Phase transformations during cooling in $\alpha+\beta$ titanium alloys. *Mater. Sci. Eng. A* **1998**, *243*, 206–211. [CrossRef]
40. Gil, F.J.; Planell, J.A. Behaviour of normal grain growth kinetics in single phase titanium and titanium alloys. *Mater. Sci. Eng. A* **2000**, *283*, 17–24. [CrossRef]